SpezialForschungsBereich F 32

Karl–Franzens Universität Graz
Technische Universität Graz
Medizinische Universität Graz

Elastic image registration in presence of polyconvex constraints

Marcus Wagner

SFB-Report No. 2010–033 September 2010

A–8010 GRAZ, HEINRICHSTRASSE 36, AUSTRIA

Supported by the
Austrian Science Fund (FWF)

Der Wissenschaftsfonds.

SFB sponsors:

- **Austrian Science Fund** (FWF)
- **University of Graz**
- **Graz University of Technology**
- **Medical University of Graz**
- **Government of Styria**
- **City of Graz**

Elastic image registration in presence of polyconvex constraints

Marcus Wagner

1. Introduction.

The present paper is concerned with the problem of image registration: [01] A given pair of greyscale images, which will be described through functions $I_0(s)$, $I_1(s)\colon \Omega \to [\,0\,,\,1\,]$ on a rectangular domain $\Omega \subset \mathbb{R}^2$, [02] should be brought in correspondence in a best possible way by means of a vector field $x(s)\colon \Omega \to \mathbb{R}^2$ satisfying the condition $I_1(s - x(s)) \approx I_0(s)$. The information captured in x will be used, for instance, in order to understand whether certain objects pictured in I_0 and I_1 are identical or if they have been subjected to intermittent alterations.

Depending on the a priori available information about the shape of the pictured objects and their motion behaviour, very different approaches for the determination of the transformation x have been proposed in the literature. For example, assuming that only pixels with the same intensity should be mapped one to another, x has been determined as optical displacement or optical flow. [03] Other approaches comprise the determination of x as a flow governed by a Navier-Stokes equation, [04] as a solution of a Monge-Kantorovič transportation problem, [05] as a rigid transformation in a higher-dimensional space [06] or by application of level-set methods. [07] For several reasons, the registration by means of an *elastic deformation* became particularly popular. [08] Firstly, in many situations one may assume that the changes in I_1 with respect to the reference image I_0 can be attributed to an elastic deformation of the pictured objects. [09] Secondly, this approach fits the problem into the multidimensional Calculus of Variations, where the solution can be obtained by well-established numerical methods. Consequently, a large part of the literature is concerned with variational methods where x is sought as a linear-elastic [10] or hyperelastic deformation. [11] In these problems, the objective consists of a fidelity term $\big(I_1(s - x(s)) - I_0(s)\big)^2$ reflecting the minimization of the grey value difference and a regularization term, [12] which will be chosen in such a way that the Euler-

---

[01] For a detailed introduction, cf. [Modersitzki 04] and [Hintermüller/ Keeling 09].

[02] In the present investigation, we restrict ourselves to the two-dimensional case. Note that the registration problem has been considered for image data on higher-dimensional domains as well, see e. g. [Barbieri/Welk/Weickert 09] and [Pöschl/Modersitzki/Scherzer 10].

[03] See [Alvarez/Weickert/Sánchez 00], [Keeling/Ring 05], and the detailed introduction in [Aubert/Kornprobst 06], pp. 250 ff. Cf. also [Haussecker/Fleet/Jähne/Garbe/Scharr/Spies 09] and [Ruhnau/Schnörr 07] for a combination of the optical flow framework with different dynamical models.

[04] [Christensen/Rabbitt/Miller 96] and [Ruhnau/Schnörr 07].

[05] [Haker/Zhu/Tannenbaum/Angenent 04] and [Museyko/Stiglmayr/Klamroth/Leugering 09].

[06] [Breitenreicher/Schnörr 09].

[07] [Vemuri/Ye/Chen/Leonard 00].

[08] Starting with [Broit 81].

[09] This is particularly the case in medical imaging since the behaviour of human tissue is governed by hyperelastic material laws, see e. g. [Ogden 03].

[10] [Fischer/Modersitzki 03], [Haber/Modersitzki 04], [Henn/Witsch 00], [Henn/Witsch 01], [Modersitzki 04], pp. 77 ff.

[11] [Droske/Rumpf 04], [Droske/Rumpf 07], [Le Guyader/Vese 09].

[12] See [Scherzer/Grasmair/Grossauer/Haltmeier/Lenzen 09], particularly pp. 53 ff., Sect. 3 and 4, for regularization methods in image processing.

Lagrange equations of the problem describe a linear-elastic or hyperelastic deformation, respectively. For the numerical solution of the problems, most authors use indirect methods. [13)]

Following [Wagner 08], pp. 26 ff., and [Wagner 10], we study the elastic image registration problem together with state constraints as well as with restrictions for the partial derivatives of x. Thus the given variational problems will be transformed into state-constrained *multidimensional control problems* of the so-called Dieudonné-Rashevsky type. [14)] The numerical solution of the resulting optimal control problems will be obtained by an efficient direct method. [15)] In contrast to the indirect methods from the Calculus of Variations, the incorporation of additional state and control constraints produces no further difficulties within this direct approach. Let us note that, in the present investigation, we will always assume that there is an overall correlation between the greyscale intensity distributions as well as the geometrical properties of the template and reference image, thus confining ourselves to unimodal registration. [16)]

In the present paper, we focus on two situations requiring the incorporation of *polyconvex gradient constraints*. First, we will combine a uniform bound for the shear stress generated by x, i. e., a convex gradient constraint, with a restriction guaranteeing the bijectivity of the deformation on a given subregion $\Theta \subseteq \Omega$. Obviously, this can be achieved by imposing inequality constraints of the type $0 < \varepsilon_1 \leqslant \mathrm{Det}\,\big(E_2 - Jx(s)\big) \leqslant \varepsilon_2 \leqslant (+\infty)$ $(\forall)\, s \in \Theta$, i. e., by addition of a polyconvex gradient constraint. In comparison with the related papers [Haber/Modersitzki 04] and [Haber/Modersitzki 07], we agree with the "first-discretize-then-optimize"-strategy but fix the lower bound $\varepsilon_1 > 0$ in order to get a constant polyconvex body as the control set. [17)] An upper bound for $\mathrm{Det}\,\big(E_2 - Jx(s)$ is already implied by the convex gradient constraint. Consequently, in the corresponding experiments with $\Theta = \Omega$, grid tangling has been completely avoided. Compared with [Wagner 10], this could be achieved by a very acceptable price: the loss of reconstruction quality amounts to maximal 3%.

Our second goal is to embed a rigidity restriction for the deformation of a subregion Θ into the elastic registration of the whole image. As we will see in Subsect. 2.c) below, this demand results in the introduction of a polyconvex gradient constraint as well.

The structure of the paper is as follows: In *Section 2*, we establish the variational as well as the optimal control formulation of the elastic image registration problem, relying on generic models of linear elasticity/hyperelasticity. Further, the additionally introduced constraints will be discussed in detail. *Section 3* is devoted to the strategy for the numerical solution of the problems. In order to justify the application of direct methods, we start with the proof of existence theorems. Then we describe the discretization of the problems, the algorithm used for the solution, as well as the visualization and evaluation of the numerical results. *Section 4* starts with the documentation of the image data used in our experiments. Then we present selected results of our numerical experiments with volumetric constraints and with the rigid motion of a subregion. Finally, in *Section 5*, we provide a discussion of the results and a conclusion.

[13)] Summarized in [Modersitzki 04], pp. 101 ff. On the contrary, [Modersitzki 09] is concerned with direct solution methods.

[14)] Different problems of mathematical image processing may be reformulated in this way. See [Brune/Maurer/Wagner 09] (optical flow with simultaneous edge detection), [Franek/Franek/Maurer/Wagner 10] (image denoising with simultaneous edge detection), [Wagner 09], pp. 564 ff., Sect. 5 (shape from shading), and the upcoming diploma thesis of Angelov (multimodal image matching).

[15)] Cf. again [Brune/Maurer/Wagner 09] and [Franek/Franek/Maurer/Wagner 10].

[16)] If one cannot expect a correspondence between the greyscale intensities of I_0 and I_1 from the outset, one arrives at the problem of multimodal registration, which must exclusively be based on the geometrical information contained in the images. Cf. [Modersitzki 09], pp. 97 ff.

[17)] In the algorithm [Haber/Modersitzki 07], p. 367 f., ε_1 has been treated as a barrier parameter with iteratively decreasing values.

Notations.

Let $\Omega \subset \mathbb{R}^m$ be the closure of a bounded Lipschitz domain (in strong sense). Then $C^k(\Omega, \mathbb{R}^r)$ denotes the space of r-dimensional vector functions $f\colon \Omega \to \mathbb{R}^r$, whose components are continuous ($k = 0$) or k-times continuously differentiable ($k = 1, \ldots, \infty$), respectively; $L^p(\Omega, \mathbb{R}^r)$ denotes the space of r-dimensional vector functions $f\colon \Omega \to \mathbb{R}^r$, whose components are integrable in the pth power ($1 \leqslant p < \infty$) or are measurable and esentially bounded ($p = \infty$). $W_0^{1,p}(\Omega, \mathbb{R}^r)$ denotes the Sobolev space of r-dimensional vector functions $f\colon \Omega \to \mathbb{R}^r$ with compactly supported components, possessing first-order weak partial derivatives and belonging together with them to the space $L^p(\Omega, \mathbb{R})$ ($1 \leqslant p < \infty$). $W_0^{1,\infty}(\Omega, \mathbb{R}^r)$ is understood as the Sobolev space of all r-vector functions $f\colon \Omega \to \mathbb{R}^r$ with Lipschitz continuous components and boundary values zero. [18] Jx denotes the Jacobi matrix of the vector function $x \in W_0^{1,p}(\Omega, \mathbb{R}^r)$. The abbreviation "$(\forall)\, s \in \mathrm{A}$" has to be read as "for almost all $s \in \mathrm{A}$" or "for all $s \in \mathrm{A}$ except a Lebesgue null set", and the symbol $\mathfrak{o}$ denotes, depending on the context, the zero element or the zero function of the underlying space. For the sake of completeness, we quote the definitions of polyconvexity for functions and sets:

Definition 1.1. *1)* **(Polyconvex functions)** [19] *We consider the elements $v \in \mathbb{R}^{nm}$ as (n,m)-matrices and collect all subdeterminants of v within a vector $T(v)$ with dimension $\tau(n,m)$. A function $r\colon \mathbb{R}^{nm} \to \mathbb{R} \cup \{\,(+\infty\,\}$ is said to be polyconvex if there exists a convex function $h\colon \mathbb{R}^{\tau(n,m)} \to \mathbb{R} \cup \{\,(+\infty\,\}$, which allows the following representation of the function r as a composition:*

$$r(v) \,=\, h(\,T(v)) \quad \forall\, v \in \mathbb{R}^{nm}\,. \tag{1.1}$$

2) **(Polyconvex sets)** [20] *Analogously, a set $\mathrm{P} \subseteq \mathbb{R}^{nm}$ is called polyconvex if there exists a convex set $\mathrm{H} \subseteq \mathbb{R}^{\tau(n,m)}$, which allows to represent the set P in the following way:*

$$\mathrm{P} \,=\, \{\, v \in \mathbb{R}^{nm} \;\big|\; T(v) \in \mathrm{H}\,\}\,. \tag{1.2}$$

Note that every convex set is polyconvex as well. Famous examples of polyconvex sets are the groups $GL^+(n) = \{\, v \in \mathbb{R}^{n\times n} \;\big|\; \mathrm{Det}\,(v) > 0\,\}$ and $SO(n) = \{\, v \in \mathbb{R}^{n\times n} \;\big|\; \mathrm{Det}\,(v) = 1\,\}$.

2. An optimal control approach to the image registration problem.

a) Variational problems corresponding with generic elasticity models.

Starting with the variational formulation of the elastic/hyperelastic image registration problem, let us consider the following variational problems within Sobolev spaces, both based on generic elasticity models. If the regularization term corresponds with a linear-elastic model, the problem reads as [21]

$$(\mathrm{V})_{lin}\colon \quad F(x) = \int_\Omega \Big(\, I_1(\,s - x(s)\,) - I_0(s)\Big)^2\, ds \,+\, \mu \cdot \int_\Omega \sum_{i,j=1}^{2} \Big(\, \frac{\partial x_i(s)}{\partial s_j} \,+\, \frac{\partial x_j(s)}{\partial s_i}\,\Big)^2 ds \;\longrightarrow\; \inf!\,; \tag{2.1}$$

$$x \in W_0^{1,p}(\Omega, \mathbb{R}^2) \tag{2.2}$$

---

[18] Cf. [Evans/Gariepy 92], p. 131, Theorem 5.

[19] [Dacorogna 08], p. 157, Definition 5.1., (iii). See also [Ball 77].

[20] See [Dacorogna 08], pp. 315 ff., and [Dacorogna/Ribeiro 06].

[21] Cf. [Henn/Witsch 01], p. 1079 f.

while a generic hyperelastic model leads to the problem [22)]

$$(\mathrm{V})_{hyp}\colon \quad F(x) = \int_\Omega \Big(I_1(\,s - x(s)\,) - I_0(s) \Big)^2 \, ds \; + \; \mu \cdot \int_\Omega \Big(c_1 \, \big\| \, E_2 - Jx(s) \, \big\|^{\,p} + c_2 \, \big(\mathrm{Det}\,(\,E_2 - Jx(s)\,)\,\big)^2 \Big) \, ds \; \longrightarrow \; \inf! \,; \tag{2.3}$$

$$x \in W_0^{1,p}(\Omega, \mathbb{R}^2)\,. \tag{2.4}$$

The image data $I_0(s)$, $I_1(s)\colon \Omega \to [\,0\,,\,1\,]$ are measurable and bounded; we assume further $2 \leqslant p < \infty$, $\mu > 0$ and $c_1,\, c_2 > 0$. E_2 denotes the $(2,2)$-unit matrix. As matrix norm, we use $\| M \| = \mathrm{trace}\,(\,M^{\mathrm{T}} M\,)$. Following [Wagner 10], we replace in both problems the integrand within the fidelity term by

$$\Big(I_1(\,s - x(s)\,) - I_0(s) \Big)^2 \approx \Big(I_1(s) \, - \, DI_1(s)^{\mathrm{T}}\, x(s) \, + \, \tfrac{1}{2}\, x(s)^{\mathrm{T}}\, D^2 I_1(s)\, x(s) \, + \, \tfrac{1}{6}\, y(s) \cdot \| \, x(s) \, \|^3 \, - \, I_0(s) \Big)^2 \tag{2.5}$$

where $DI_1 \in L^\infty(\Omega, \mathbb{R}^2)$ and $D^2 I_1 \in L^\infty(\Omega, \mathbb{R}^{2\times 2})$ are suitable approximations for the derivatives ∇I_1 and $\nabla^2 I_1$ within a second-order Taylor expansion of $I_1(\,s - x(s)\,)$. The third-order remainder term $\frac{1}{6}\, y(s) \cdot \| \, x(s) \, \|^3$ contains an additional, state-constrained variable $y \in L^\infty(\Omega, \mathbb{R})$, $|\, y(s) \,| \leqslant \eta_{max}$. [23)] Note that the integrand within (2.4) is a polyconvex function [24)] with respect to the derivatives of x. Below, we will further deviate from convexity of the problem by introducing polyconvex *constraints* as well.

b) Optimal control reformulation by incorporation of a convex gradient constraint.

From the viewpoint of elasticity, the variational models are incomplete since they contain no bound for the resulting shear stress, which is proportional to the modulus of Jx. [25)] On the other hand, the introduction of an additional control restriction leads to a further regularization of the problems, which is particularly desirable for the treatment of polyconvex constraints. Consequently, to both variational problems $(\mathrm{V})_{lin}$ and $(\mathrm{V})_{hyp}$, the convex gradient constraint

$$Jx(s) \; \in \; \mathrm{K} \; \subset \; \mathbb{R}^{2\times 2} \quad (\forall)\, s \in \Omega \tag{2.6}$$

where $\mathrm{K} \subset \mathbb{R}^{2\times 2}$ is a convex norm body with $\mathfrak{o} \in \mathrm{int}\,(\mathrm{K})$, will be added. In the numerical experiments below, we will specify K as the four-dimensional cube $\mathrm{K} = [\,-R\,,\,R\,]^4$ with $R > 0$.

c) Incorporation of polyconvex gradient constraints.

We are now in position to describe two situations, which lead to the introduction of polyconvex gradient constraints:

1) Bijective deformation of a subregion. The bijectivity of the variable transformation $\tilde{s} = s - x(s)$ on the subregion $\Theta \subseteq \Omega$ is ensured while there are no changes of the sign of its Jacobian on Θ. This situation will be described by the polyconvex gradient constraint $\mathrm{Det}\,\big(\,E_2 - Jx(s)\,\big) > 0$ or

$$\mathrm{Det}\,\big(\,E_2 - Jx(s)\,\big) \; - \; \varepsilon_1 \; \geqslant \; 0 \quad (\forall)\, s \in \Theta \tag{2.7}$$

[22)] [Droske/Rumpf 04], p. 673 f.

[23)] [Wagner 10], p. 4.

[24)] See Definition 1.1. above.

[25)] We emphasize that the validity of the underlying elasticity models is bound by restrictions for the maximal shear stress generated by the deformation x. See, e. g. [Chmelka/Melan 76], pp. 38 – 45 (linear-elastic model, material sciences) and [Gasser/Holzapfel 02], p. 340 f., and the literature cited there (different hyperelastic models, human tissue).

with sufficiently small $\varepsilon_1 > 0$. More generally, the allowed change of a volume element may be bounded by the two-sided constraint [26)]

$$0 < \varepsilon_1 \leqslant \mathrm{Det}\big(E_2 - Jx(s)\big) \leqslant \varepsilon_2 < \infty \quad (\forall)\, s \in \Theta \iff \mathrm{Det}\big(E_2 - Jx(s)\big) - \varepsilon_1 \geqslant 0\,,\ \mathrm{Det}\big(E_2 - Jx(s)\big) - \varepsilon_2 \leqslant 0 \quad (\forall)\, s \in \Theta\,. \tag{2.8}$$

Note that already the convex constraint (2.6) implies an upper bound for $\mathrm{Det}\big(E_2 - Jx(s)\big)$.

2) Subregions subjected to a rigid deformation. In this case, on the subregion $\Theta \subseteq \Omega$ it holds that $s - x(s) = R\,s - s_0$ with $R = \left(\begin{smallmatrix}\cos\alpha & -\sin\alpha \\ \sin\alpha & \cos\alpha\end{smallmatrix}\right)$. This implies $\mathrm{Det}\,(R) = \mathrm{Det}\,\big(E_2 - Jx(s)\big) = 1$ as well as $Jx(s) = E_2 - R = \textit{const.} \iff \nabla^2 x_1(s) = \mathfrak{o}$, $\nabla^2 x_2(s) = \mathfrak{o}$. Consequently, we obtain a polyconvex gradient constraint

$$1 - \varepsilon \leqslant \mathrm{Det}\,(E_2 - Jx(s)) \leqslant 1 + \varepsilon \quad (\forall)\, s \in \Theta \iff \tag{2.9}$$

$$-\varepsilon \leqslant \mathrm{Det}\big(Jx(s)\big) - \frac{\partial}{\partial s_1} x_1(s) - \frac{\partial}{\partial s_2} x_2(s) \leqslant \varepsilon \quad (\forall)\, s \in \Theta \tag{2.10}$$

together with the following convex constraints for the second partial derivatives of x:

$$\frac{\partial^2}{\partial s_1^2} x_i(s)\,,\ \frac{\partial^2}{\partial s_1\,\partial s_2} x_i(s)\,,\ \frac{\partial^2}{\partial s_2^2} x_i(s) \in [\,-\varepsilon\,,\,\varepsilon\,] \quad (\forall)\, s \in \Theta\,,\ i = 1,\,2 \tag{2.11}$$

where $\varepsilon > 0$ is sufficiently small.

d) The resulting control problems.

To $(\mathrm{V})_{lin}$ and $(\mathrm{V})_{hyp}$, we add the convex gradient restriction (2.6), thus converting both problems into multidimensional control problems of Dieudonné-Rashevsky type. Further, the integrand within the fidelity term will be replaced by its approximation (2.5) where y will be specified as a measurable function, which is uniformly bounded by η_{max}. As a result, we obtain the following state-constrained optimal control problems:

$$(\mathrm{P})_{lin}\colon \quad F(x,y) = \int_\Omega \Big(I_1(s) - DI_1(s)^{\mathrm{T}}\, x(s) + \tfrac{1}{2}\, x(s)^{\mathrm{T}}\, D^2 I_1(s)\, x(s) + \tfrac{1}{6}\, y(s)\, \|\, x(s)\,\|^3 - I_0(s) \Big)^2\, ds$$

$$+\ \mu \cdot \int_\Omega \sum_{i,j=1}^{2} \Big(\frac{\partial x_i(s)}{\partial s_j} + \frac{\partial x_j(s)}{\partial s_i} \Big)^2\, ds \longrightarrow \inf\!\,; \tag{2.12}$$

$$(x,y) \in W_0^{1,p}(\Omega, \mathbb{R}^2) \times L^\infty(\Omega, \mathbb{R})\,; \tag{2.13}$$

$$|\, y(s)\,| \leqslant \eta_{max} \ (\forall)\, s \in \Omega\,; \tag{2.14}$$

$$Jx(s) \in \mathrm{K} \ (\forall)\, s \in \Omega \tag{2.15}$$

(linear-elastic image registration) and

$$(\mathrm{P})_{hyp}\colon \quad F(x,y) = \int_\Omega \Big(I_1(s) - DI_1(s)^{\mathrm{T}}\, x(s) + \tfrac{1}{2}\, x(s)^{\mathrm{T}}\, D^2 I_1(s)\, x(s) + \tfrac{1}{6}\, y(s)\, \|\, x(s)\,\|^3 - I_0(s) \Big)^2\, ds$$

$$+\ \mu \cdot \int_\Omega \Big(c_1\, \big\|\, E_2 - Jx(s)\,\big\|^{\,p} + c_2\, \big(\mathrm{Det}\,(\,E_2 - Jx(s)\,)\big)^2 \Big)\, ds \longrightarrow \inf\!\,; \tag{2.16}$$

$$(x,y) \in W_0^{1,p}(\Omega, \mathbb{R}^2) \times L^\infty(\Omega, \mathbb{R})\,; \tag{2.17}$$

$$|\, y(s)\,| \leqslant \eta_{max} \ (\forall)\, s \in \Omega\,; \tag{2.18}$$

$$Jx(s) \in \mathrm{K} \ (\forall)\, s \in \Omega \tag{2.19}$$

[26)] Cf. [Haber/Modersitzki 07], p. 363, (6b).

(hyperelastic image registration) with measurable, bounded data I_0, $I_1 \in L^\infty(\Omega, \mathbb{R})$, $DI_1 \in L^\infty(\Omega, \mathbb{R}^2)$ and $D^2 I_1 \in L^\infty(\Omega, \mathbb{R}^{2\times 2})$, $1 \leqslant p < \infty$, an uniform bound $\eta_{max} > 0$ for the fitting variable y in the remainder in the Taylor expansion, a regularization parameter $\mu > 0$ and positive weights c_1, $c_2 > 0$. $\mathrm{K} \subset \mathbb{R}^{2\times 2}$ is a convex body with $\mathfrak{o} \in \mathrm{int}\,(\mathrm{K})$.
The incorporation of the polyconvex constraints (2.7) or (2.8) into $(\mathrm{P})_{lin}$ and $(\mathrm{P})_{hyp}$ leads to the problems $(\mathrm{P})_{lin}{}^{(1)}$ and $(\mathrm{P})_{hyp}{}^{(1)}$, which are identical with the former but the control restriction

$$Jx(s) \,\in\, \mathrm{K} \cap \mathrm{P} \;\; (\forall)\, s \in \Theta \tag{2.20}$$

with

$$\mathrm{P} \,=\, \big\{\, v \in \mathbb{R}^{2\times 2} \;\big|\; \mathrm{Det}\,(E_2 - v) - \varepsilon_1 \geqslant 0 \,\big\} \quad \text{or} \tag{2.21}$$

$$\mathrm{P} \,=\, \big\{\, v \in \mathbb{R}^{2\times 2} \;\big|\; \mathrm{Det}\,(E_2 - v) - \varepsilon_1 \geqslant 0\,,\; \mathrm{Det}\,(E_2 - v) - \varepsilon_2 \leqslant 0 \,\big\}\,, \tag{2.22}$$

respectively, has been added. Note that $\mathrm{K} \cap \mathrm{P} \subset \mathbb{R}^{2\times 2}$ is a polyconvex, compact, arcwise connected set [27] with nonempty interior.
For the consideration of the constraints (2.9) and (2.11), the following reformulation of $(\mathrm{P})_{lin}$ must be done:

$$\begin{aligned}(\mathrm{P})_{lin}{}^{(2)}\colon\quad F(w, x_1, x_2, y) = \int_\Omega \Big(& I_1(s) \,-\, DI_1(s)^{\mathrm{T}}\, w(s) \,+\, \tfrac{1}{2}\, w(s)^{\mathrm{T}}\, D^2 I_1(s)\, w(s) \,+\, \tfrac{1}{6}\, y(s)\, \|\, w(s)\, \|^3 \\ & - I_0(s) \Big)^2 \, ds \,+\, 2\,\mu \cdot \int_\Omega \Big(2\, x_{11}(s)^2 + \big(x_{12}(s) + x_{21}(s) \big)^2 + 2\, x_{22}(s)^2 \Big)\, ds \;\longrightarrow\; \inf!\,; \end{aligned} \tag{2.23}$$

$$(w, x_1, x_2, y) \in W_0^{1,p}(\Omega, \mathbb{R}^2) \,\times\, L^p(\Omega, \mathbb{R}^2) \,\times\, L^p(\Omega, \mathbb{R}^2) \,\times\, L^\infty(\Omega, \mathbb{R})\,;\;\; x_1 \,\big|\, \Theta\,,\;\; x_2 \,\big|\, \Theta \in W^{1,p}(\Theta, \mathbb{R}^2)\,; \tag{2.24}$$

$$\nabla w_1(s) \,=\, x_1(s)\,,\;\; \nabla w_2(s) \,=\, x_2(s) \quad (\forall)\, s \in \Omega\,; \tag{2.25}$$

$$|\, y(s) \,| \,\leqslant\, \eta_{max} \;\; (\forall)\, s \in \Omega\,; \tag{2.26}$$

$$\begin{pmatrix} x_{11}(s) & x_{12}(s) \\ x_{21}(s) & x_{22}(s) \end{pmatrix} \,\in\, \mathrm{K} \;\; (\forall)\, s \in \Omega\,; \tag{2.27}$$

$$\begin{pmatrix} x_{11}(s) & x_{12}(s) \\ x_{21}(s) & x_{22}(s) \end{pmatrix} \,\in\, \mathrm{K} \cap \mathrm{P} \,=\, \mathrm{K} \cap \big\{\, v \in \mathbb{R}^{2\times 2} \;\big|\; |\, \mathrm{Det}\,(v) - v_{11} - v_{22} \,| \leqslant \varepsilon \,\big\} \quad (\forall)\, s \in \Theta\,; \tag{2.28}$$

$$Jx_1(s)\,,\;\; Jx_2(s) \,\in\, \widetilde{\mathrm{K}} \,=\, \big\{\, v \in \mathbb{R}^{2\times 2} \;\big|\; \mathrm{Max}_{i,j}\, |\, v_{ij} \,| \,\leqslant\, \varepsilon \,\big\} \quad (\forall)\, s \in \Theta \tag{2.29}$$

where $\varepsilon > 0$. In $(\mathrm{P})_{lin}{}^{(2)}$, the restriction $Jw \in \mathrm{K} \cap \mathrm{P}$ forms a polyconvex state constraint on Θ. As remarked in [Wagner 10], p. 5 f., Remark 1, because of $\mathfrak{o} \in \mathrm{int}\,(\mathrm{K})$, the problem $(\mathrm{P})_{lin}{}^{(2)}$ admits certain feasible rigid motions. Accordingly, a problem $(\mathrm{P})_{hyp}{}^{(2)}$ will be obtained as a reformulation of $(\mathrm{P})_{hyp}$.

3. Numerical solution by direct methods.

a) Existence theorems.

In order to justify the application of direct methods to the solution of the multidimensional control problems from Subsection 2.d), the existence of global minimizers must be first ensured. Concerning $(\mathrm{P})_{lin}$ and $(\mathrm{P})_{hyp}$, we may refer to the existence theorems from [Wagner 10], which will be summarized in the following

Theorem 3.1. [28] *Consider the problems* $(\mathrm{P})_{lin}$ *and* $(\mathrm{P})_{hyp}$ *with the assumptions about the data mentioned above.*

[27] The last assertion follows from [Berger 04], p. 165, Corollary 8.4.3.

[28] [Wagner 10], p. 6, Theorem 2.1., and p. 7 f., Theorem 2.2.

1) Assume that a sequence $\{\,(x^N, y^N)\,\}$ *of feasible processes of* $(\mathrm{P})_{lin}$ *obeys the convergence relations*

$$x^N \to^{C^0(\Omega,\mathbb{R}^2)} x\,, \quad Jx^N \overset{*}{\rightharpoonup}^{L^\infty(\Omega,\mathbb{R}^4)} Jx \quad \text{and} \quad y^N \overset{*}{\rightharpoonup}^{L^\infty(\Omega,\mathbb{R})} y\,. \tag{3.1}$$

Then (x, y) *is feasible as well. Furthermore, the objective* (2.12) *is bounded from below and lower semicontinuous with respect to the convergence from* (3.1)*, and* $(\mathrm{P})_{lin}$ *admits a global minimizer* $(\hat{x}, \hat{y}) \in W_0^{1,\infty}(\Omega, \mathbb{R}^2) \times L^\infty(\Omega, \mathbb{R})$*.*

2) For $(\mathrm{P})_{hyp}$*, the same assertions are true.*

We may now state our first existence theorem:

Theorem 3.2. (Existence of global minimizers for problems with volumetric constraints) *Consider the problems* ${(\mathrm{P})_{lin}}^{(1)}$ *and* ${(\mathrm{P})_{hyp}}^{(1)}$ *with the assumptions about the data mentioned above. Assume further that* $\Theta \subseteq \Omega$ *is a compact subset with nonempty interior.*

1) Whether the polyconvex set in (2.20) *is described by* (2.21) *or* (2.22)*,* ${(\mathrm{P})_{lin}}^{(1)}$ *admits a global minimizer* $(\hat{x}, \hat{y}) \in W_0^{1,\infty}(\Omega, \mathbb{R}^2) \times L^\infty(\Omega, \mathbb{R})$*.*

2) Assertion 1) remains true for ${(\mathrm{P})_{hyp}}^{(1)}$ *as well.*

Proof. 1) Due to the facts that the zero solution remains feasible after adding the restriction (2.20) to $(\mathrm{P})_{lin}$ and $F(x, y) \geqslant 0$, the new problem ${(\mathrm{P})_{lin}}^{(1)}$ admits a minimizing sequence $\{\,(x^N, y^N)\,\}$ as well. Since (2.14) and (2.15), the norms $\|\,x^N\,\|_{W_0^{1,\infty}(\Omega,\mathbb{R}^2)}$ as well as $\|\,y^N\,\|_{L^\infty(\Omega,\mathbb{R})}$ remain bounded, and after a passage to appropriate subsequences, we may assume that the minimizing sequence possesses a limit element $(\hat{x}, \hat{y}) \in W_0^{1,\infty}(\Omega, \mathbb{R}^2) \times L^\infty(\Omega, \mathbb{R})$, which is, by Theorem 3.1., feasible in $(\mathrm{P})_{lin}$. Consequently, it only remains to check whether $\hat{x}$ satisfies the constraint (2.20). From [Dacorogna 08], p. 395, Theorem 8.20. 1), and p. 396, Remark 8.21., (v), the following implications may be derived:

$$x^N \overset{*}{\rightharpoonup}^{W^{1,\infty}(\Omega,\mathbb{R}^2)} \hat{x} \implies (x^N \,|\, \Theta) \overset{*}{\rightharpoonup}^{W^{1,\infty}(\Theta,\mathbb{R}^2)} (\hat{x} \,|\, \Theta) \implies \tag{3.2}$$

$$\big(\,(E_2 - Jx^N)\,\big|\,\Theta\,\big) \overset{*}{\rightharpoonup}^{L^\infty(\Theta,\mathbb{R}^4)} \big(\,(E_2 - J\hat{x})\,\big|\,\Theta\,\big) \implies \tag{3.3}$$

$$\big(\,\mathrm{Det}\,\big(\,E_2 - Jx^N\,\big)\,\big|\,\Theta\,\big) \overset{*}{\rightharpoonup}^{L^\infty(\Theta,\mathbb{R})} \big(\,\mathrm{Det}\,\big(\,E_2 - J\hat{x}\,\big)\,\big|\,\Theta\,\big)\,, \tag{3.4}$$

and we arrive at

$$\lim_{N\to\infty} \langle\,\mathrm{Det}\,\big(\,E_2 - Jx^N\,\big) - \varepsilon_1\,,\,\varphi\,\rangle = \langle\,\mathrm{Det}\,\big(\,E_2 - J\hat{x}\,\big) - \varepsilon_1\,,\,\varphi\,\rangle \tag{3.5}$$

for all test functions $\varphi \in L^1(\Theta, \mathbb{R})$ with $\varphi(s) \geqslant 0$ $(\forall)\, s \in \Theta$. Consequently, the inequality $\mathrm{Det}\,\big(\,E_2 - J\hat{x}(s)\,\big) - \varepsilon_1 \geqslant 0$ holds almost everywhere on Θ. For the second inequality in (2.8), we reason in a completely analogous way. Now, we invoke Theorem 3.1. again in order to confirm the lower semicontinuity of the objective, and the proof is complete.

2) This assertion may be proven in complete analogy to Part 1). ∎

In a similar way, we obtain an existence theorem for the problems ${(\mathrm{P})_{lin}}^{(2)}$ and ${(\mathrm{P})_{hyp}}^{(2)}$:

Theorem 3.3. (Existence of global minimizers for problems with constraints describing a rigid motion) *Consider the problems* ${(\mathrm{P})_{lin}}^{(2)}$ *and* ${(\mathrm{P})_{hyp}}^{(2)}$ *with the assumptions about the data mentioned above, and assume further that* $\Theta \subseteq \Omega$ *is a compact set with nonempty interior.*

1) Then the problem ${(\mathrm{P})_{lin}}^{(2)}$ *admits a global minimizer* $(\hat{w}, \hat{x}, \hat{y}) \in W_0^{1,\infty}(\Omega, \mathbb{R}^2) \times L^\infty(\Omega, \mathbb{R}^4) \times L^\infty(\Omega, \mathbb{R})$ *with* $(\hat{x} \,|\, \Theta) \in W^{1,\infty}(\Theta, \mathbb{R}^4)$*.*

2) The problem $(\mathrm{P})_{hyp}{}^{(2)}$ *admits a global minimizer* $(\hat{w},\hat{x},\hat{y}) \in W_0^{1,\infty}(\Omega,\mathbb{R}^2) \times L^\infty(\Omega,\mathbb{R}^4) \times L^\infty(\Omega,\mathbb{R})$ *with* $(\hat{x}\,|\,\Theta) \in W^{1,\infty}(\Theta,\mathbb{R}^4)$ *as well.*

Proof. 1) Since $F(w,x_1,x_2,y) \geqslant 0$ and the zero solution is feasible, $(\mathrm{P})_{lin}{}^{(2)}$ admits a minimizing sequence $\{\,(w^N,x_1^N,x_2^N,y^N)\,\}$ wherein, by (2.26) and (2.27), $\|\,w^N\,\|_{W_0^{1,\infty}(\Omega,\mathbb{R}^2)}$ as well as $\|\,y^N\,\|_{L^\infty(\Omega,\mathbb{R})}$ remain bounded. (2.29) implies the boundedness of $\|\,(x_1^N\,|\,\Theta)\,\|_{W_0^{1,\infty}(\Theta,\mathbb{R}^4)}$ and $\|\,(x_2^N\,|\,\Theta)\,\|_{W_0^{1,\infty}(\Theta,\mathbb{R}^4)}$. After a passage to suitable subsequences, we may assume that the minimizing sequence possesses a limit element $(\hat{w},\hat{x}_1,\hat{x}_2,\hat{y}) \in W_0^{1,\infty}(\Omega,\mathbb{R}^2) \times L^\infty(\Omega,\mathbb{R}^2) \times L^\infty(\Omega,\mathbb{R}^2) \times L^\infty(\Omega,\mathbb{R})$ with $(\hat{x}_1\,|\,\Theta)$, $(\hat{x}_2\,|\,\Theta) \in W^{1,\infty}(\Omega,\mathbb{R}^2)$ and

$$w^N \to^{C^0(\Omega,\mathbb{R}^2)} \hat{w}\,,\;\; x_1^N \overset{*}{\rightharpoonup}{}^{L^\infty(\Omega,\mathbb{R}^2)} \hat{x}_1\,,\;\; x_2^N \overset{*}{\rightharpoonup}{}^{L^\infty(\Omega,\mathbb{R}^2)} \hat{x}_2\,,\;\; y^N \overset{*}{\rightharpoonup}{}^{L^\infty(\Omega,\mathbb{R})} \hat{y}\,, \tag{3.6}$$

$$(x_1^N\,|\,\Theta) \to^{C^0(\Theta,\mathbb{R}^2)} (\hat{x}_1\,|\,\Theta)\,,\;\; (x_2^N\,|\,\Theta) \to^{C^0(\Theta,\mathbb{R}^2)} (\hat{x}_2\,|\,\Theta)\,, \tag{3.7}$$

$$(Jx_1^N\,|\,\Theta) \overset{*}{\rightharpoonup}{}^{L^\infty(\Theta,\mathbb{R}^4)} (J\hat{x}_1\,|\,\Theta)\,,\;\; (Jx_2^N\,|\,\Theta) \overset{*}{\rightharpoonup}{}^{L^\infty(\Omega,\mathbb{R}^4)} (J\hat{x}_2\,|\,\Theta)\,. \tag{3.8}$$

Under the weak*-convergence of $\{\,y^N\,\}$ and $\{\,Jw^N\,\} = \{\,(x_1^N,x_2^N)\,\}$, the convex restrictions (2.26) and (2.27) will be conserved; due to the uniform convergence of $\{\,x_1^N\,\}$ and $\{\,x_2^N\,\}$ on Θ, the limit element obeys the state constraint (2.28), and under the weak*-convergence of $\{\,Jx_1^N\,\}$ and $\{\,Jx_2^N\,\}$ within $L^\infty(\Theta,\mathbb{R}^4)$, the gradient restrictions (2.29) will be carried over to the limit element. As a consequence, $(\hat{w},\hat{x}_1,\hat{x}_2,\hat{y})$ is feasible in $(\mathrm{P})_{lin}{}^{(2)}$, and in complete analogy to Theorem 3.2., 1), we see that the limit element is a global minimizer.

2) Part 2) will be proven analogously to Part 1). ∎

b) Discretization and solution strategy.

Our strategy for the numerical solution of the optimal control problems $(\mathrm{P})_{lin}{}^{(k)}$ and $(\mathrm{P})_{hyp}{}^{(k)}$ is based on the principle "first discretize, then optimize". For the discretization of the problems, which is adapted on a regular triangulation of the rectangular domain Ω,[29] we refer to [Wagner 10], p. 8 f. Let us describe, however, the discretization of the control restrictions with $\mathrm{K} = [\,-R\,,\,R\,]$, $\widetilde{\mathrm{K}} = [\,-\varepsilon\,,\,\varepsilon\,]$ and P according to (2.21) and (2.28) in more detail. Assuming that the square $\mathrm{Q}_{k,l}$ with edge length 1 is divided into the adjacent triangles $\Delta'_{k,l} = \Delta(s_{k-1,l-1},s_{k,l-1},s_{k,l})$ and $\Delta''_{k,l} = \Delta(s_{k-1,l-1},s_{k,l},s_{k-1,l})$, and that $\xi_{k,l}^{(i)} = x_i(s_{k,l})$, $i = 1,\,2$, in the grid points $s_{k,l}$, we obtain as the discretization of (2.15) and (2.19):

$$-R \leqslant \xi_{k,l-1}^{(i)} - \xi_{k-1,l-1}^{(i)} \leqslant R\,,\;\; -R \leqslant \xi_{k,l}^{(i)} - \xi_{k,l-1}^{(i)} \leqslant R \text{ on } \Delta'_{k,l}\,; \tag{3.9}$$

$$-R \leqslant \xi_{k,l}^{(i)} - \xi_{k-1,l}^{(i)} \leqslant R\,,\;\; -R \leqslant \xi_{k-1,l}^{(i)} - \xi_{k-1,l-1}^{(i)} \leqslant R \text{ on } \Delta''_{k,l} \tag{3.10}$$

for all $\mathrm{Q}_{k,l} \subset \Omega$ and $i = 1,\,2$. To discretize (2.20) means then to add the restrictions

$$\varepsilon_1 \leqslant \big(1-(\,\xi_{k,l-1}^{(1)} - \xi_{k-1,l-1}^{(1)}\,)\big)\big(1-(\,\xi_{k,l}^{(2)} - \xi_{k,l-1}^{(2)}\,)\big) - \big(\xi_{k,l}^{(1)} - \xi_{k,l-1}^{(1)}\big)\big(\xi_{k,l-1}^{(2)} - \xi_{k-1,l-1}^{(2)}\big) \leqslant \varepsilon_2 \text{ on } \Delta'_{k,l}\,; \tag{3.11}$$

$$\varepsilon_1 \leqslant \big(1-(\,\xi_{k,l}^{(1)} - \xi_{k-1,l}^{(1)}\,)\big)\big(1-(\,\xi_{k-1,l}^{(2)} - \xi_{k-1,l-1}^{(2)}\,)\big) - \big(\xi_{k-1,l}^{(1)} - \xi_{k-1,l-1}^{(1)}\big)\big(\xi_{k,l}^{(2)} - \xi_{k-1,l}^{(2)}\big) \leqslant \varepsilon_2 \text{ on } \Delta''_{k,l} \tag{3.12}$$

for all $\mathrm{Q}_{k,l} \subset \Theta$. Accordingly, with $\omega_{k,l}^{(i)} = w(s_{k,l})$ in the grid points $s_{k,l}$, we discretize (2.27) by

$$-R \leqslant \omega_{k,l-1}^{(i)} - \omega_{k-1,l-1}^{(i)} \leqslant R\,,\;\; -R \leqslant \omega_{k,l}^{(i)} - \omega_{k,l-1}^{(i)} \leqslant R \text{ on } \Delta'_{k,l}\,; \tag{3.13}$$

$$-R \leqslant \omega_{k,l}^{(i)} - \omega_{k-1,l}^{(i)} \leqslant R\,,\;\; -R \leqslant \omega_{k-1,l}^{(i)} - \omega_{k-1,l-1}^{(i)} \leqslant R \text{ on } \Delta''_{k,l} \tag{3.14}$$

[29] Note that the necessity to use *triangular* elements for the discretization of problems involving conditions (2.7) or (2.8) has been pointed out in [Haber/Modersitzki 07], p. 364 f., as well.

for all $Q_{k,l} \subset \Omega$, $i = 1, 2$, and (2.28) by

$$-\varepsilon \leqslant \left(\omega^{(1)}_{k,l-1} - \omega^{(1)}_{k-1,l-1}\right)\left(\omega^{(2)}_{k,l} - \omega^{(2)}_{k,l-1}\right) - \left(\omega^{(1)}_{k,l} - \omega^{(1)}_{k,l-1}\right)\left(\omega^{(2)}_{k,l-1} - \omega^{(2)}_{k-1,l-1}\right) - \left(\omega^{(1)}_{k,l-1} - \omega^{(1)}_{k-1,l-1}\right) - \left(\omega^{(2)}_{k,l} - \omega^{(2)}_{k,l-1}\right) \leqslant \varepsilon \text{ on } \Delta'_{k,l}\,; \quad (3.15)$$

$$-\varepsilon \leqslant \left(\omega^{(1)}_{k,l} - \omega^{(1)}_{k-1,l}\right)\left(\omega^{(2)}_{k-1,l} - \omega^{(2)}_{k-1,l-1}\right) - \left(\omega^{(1)}_{k-1,l} - \omega^{(1)}_{k-1,l-1}\right)\left(\omega^{(2)}_{k,l} - \omega^{(2)}_{k-1,l}\right) - \left(\omega^{(1)}_{k,l} - \omega^{(1)}_{k-1,l}\right) - \left(\omega^{(2)}_{k-1,l} - \omega^{(2)}_{k-1,l-1}\right) \leqslant \varepsilon \text{ on } \Delta''_{k,l} \quad (3.16)$$

for all $Q_{k,l} \subset \Theta$. Finally, (2.25) and (2.29) will be discretized by

$$\xi^{(i,1)}_{k-1,l-1} = \omega^{(i)}_{k,l-1} - \omega^{(i)}_{k-1,l-1}\,,\ \xi^{(i,2)}_{k-1,l-1} = \omega^{(i)}_{k,l} - \omega^{(i)}_{k,l-1} \text{ on } \Delta'_{k,l}\,; \quad (3.17)$$

$$\xi^{(i,1)}_{k-1,l-1} = \omega^{(i)}_{k,l} - \omega^{(i)}_{k-1,l}\,,\ \xi^{(i,2)}_{k-1,l-1} = \omega^{(i)}_{k-1,l} - \omega^{(i)}_{k-1,l-1} \text{ on } \Delta''_{k,l} \quad (3.18)$$

for all $Q_{k,l} \cap \Theta \neq \emptyset$, $i = 1, 2$, and

$$-\varepsilon \leqslant \xi^{(i,j)}_{k,l-1} - \xi^{(i,j)}_{k-1,l-1} \leqslant \varepsilon\,,\ -\varepsilon \leqslant \xi^{(i,j)}_{k,l} - \xi^{(i,j)}_{k,l-1} \leqslant \varepsilon \text{ on } \Delta'_{k,l}\,; \quad (3.19)$$

$$-\varepsilon \leqslant \xi^{(i,j)}_{k,l} - \xi^{(i,j)}_{k-1,l} \leqslant \varepsilon\,,\ -\varepsilon \leqslant \xi^{(i,j)}_{k-1,l} - \xi^{(i,j)}_{k-1,l-1} \leqslant \varepsilon \text{ on } \Delta''_{k,l} \quad (3.20)$$

for all $Q_{k,l} \subset \Theta$, $1 \leqslant i, j \leqslant 2$. The evaluation of the necessary optimality conditions (Karush-Kuhn-Tucker conditions) for the resulting large-scale nonlinear optimization problems will be effected by interior-point methods. [30] Our input/output platform for the image data was MATLAB; the discretized problem has been formulated within modelling language AMPL [31] and subsequently transferred to the interior-point solver IPOPT. [32] The results have been represented and evaluated with MATLAB again. In order to ensure the convergence of the discretization method with respect to the x-component of the solutions, one has to proceed in analogy to [Franek/Franek/Maurer/Wagner 10], p. 10, Corollary 2.7., assuming that the image data I_1 are sufficiently smooth.

c) Evaluation and visualization of numerical results.

For $(\mathrm{P})_{lin}{}^{(1)}$ and $(\mathrm{P})_{hyp}{}^{(1)}$, our main indicator for the quantitative evaluation of the results is the relative reconstruction error

$$Q(\hat{x}, \hat{y}) = \left(\frac{\displaystyle\int_{\Omega \setminus \Omega_R} \Big(I_{rek}(s) - I_0(s) \Big)^2 \, ds}{\displaystyle\int_{\Omega \setminus \Omega_R} \Big(I_1(s) \ - I_0(s) \Big)^2 \, ds} \right)^{1/2} \quad (3.21)$$

where the entering reconstruction $I_{rek}(s)$ of I_0 has been calculated as

$$I_{rek}(s) = I_1(s) - DI_1(s)^{\mathrm{T}}\,\hat{x}(s) + \tfrac{1}{2}\,\hat{x}(s)^{\mathrm{T}}\,D^2 I_1(s)\,\hat{x}(s) + \tfrac{1}{6}\,\hat{y}(s) \cdot \| \hat{x}(s) \|^3 \quad (3.22)$$

with the help of the obtained minimizing solution $(\hat{x}, \hat{y})$ of $(\mathrm{P})_{lin}{}^{(k)}$ or $(\mathrm{P})_{hyp}{}^{(k)}$. As pointed out in [Wagner 10], the influence of the member $\frac{1}{6}\,\hat{y}(s) \cdot \| \hat{x}(s) \|^3$, which can be interpreted as a grey value correction, should be controlled by means of the indicator

$$G(\hat{x}, \hat{y}) = \operatorname*{Max}_{s \in \Omega \setminus \Omega_R} \left| \tfrac{1}{6}\,\hat{y}(s) \cdot \| \hat{x}(s) \|^3 \right|. \quad (3.23)$$

[30] See, for example, [Jansen 97].

[31] [Fourer/Gay/Kernighan 03].

[32] [Laird/Wächter 09], [Wächter/Biegler 06]. The experiments have been performed with version 3.6.1., compiled with the MA27 routine.

We consider a result as practically acceptable as long as G remains below the maximal grey value difference of the original images. For the calculation of Q and G, a frame Ω_R dyed in black of 4 pixels width will be excluded. Finally, the grid deformation will be measured by the following indicator T, which is directly related to the particular discretization:

$$T(\hat{x}) = \max_{(k,l)\,:\,\mathrm{Q}_{k,l}\subset\Theta} \Big(\frac{1}{2}\cdot \mathrm{Det} \begin{pmatrix} 1-\hat{x}_1(s_{k,l-1})+\hat{x}_1(s_{k-1,l-1}) & 1-\hat{x}_1(s_{k,l})+\hat{x}_1(s_{k-1,l-1}) \\ -\hat{x}_2(s_{k,l-1})+\hat{x}_2(s_{k-1,l-1}) & 1-\hat{x}_2(s_{k,l})+\hat{x}_2(s_{k-1,l-1}) \end{pmatrix}, \\ \frac{1}{2}\cdot \mathrm{Det} \begin{pmatrix} 1-\hat{x}_1(s_{k,l})+\hat{x}_1(s_{k-1,l-1}) & -\hat{x}_1(s_{k-1,l})+\hat{x}_1(s_{k-1,l-1}) \\ 1-\hat{x}_2(s_{k,l})+\hat{x}_2(s_{k-1,l-1}) & 1-\hat{x}_2(s_{k-1,l})+\hat{x}_2(s_{k-1,l-1}) \end{pmatrix} \Big). \quad (3.24)$$

For $(\mathrm{P})_{lin}{}^{(2)}$ and $(\mathrm{P})_{hyp}{}^{(2)}$, we introduce the indicators $Q(\hat{w},\hat{y})$ and $G(\hat{w},\hat{y})$ accordingly.
The results of an elastic image registration will be visualized by a deformed grid showing the effect of the solution $\hat{x}$ when applied to a reference grid (see e. g. Fig. 14) as well as by a colorful orientation plot (see e. g. Fig. 10). [33] Here the color of a pixel encodes the direction of the deformation vector while its intensity increases with the magnitude of the vector. The correspondence between orientation and color can be read from the colored border as a legend. This visualization has been realized with a HSI color model [34] where every color is represented by the three coordinates hue, saturation and intensity. Since we need only two coordinates for the visualization of the deformation field $\hat{x}$, the saturation has been left constant.
Besides $\hat{x}$, we picture the grey value correction $\big|\, \frac{1}{6}\, \hat{y}(s)\cdot \| \hat{x}(s) \|^3 \,\big|$, where the correspondence of the greyscale values has been inverted (white corresponds to zero) and magnified by the factor 3 (see e. g. Fig. 11). In these figures, a frame of 4 pixels width has been dyed in grey.

4. Numerical experiments.

a) Description of the image data.

For our numerical experiments, three pairs of test images have been chosen. The first pair (Figs. 1 and 3) originates from medical imaging and shows a coronal section through the left kidney; moreover, in the left half of the images, a part of the spine is visible. [35] The images have been consecutively generated via MR tomography with an interval of 2.4 seconds. The original data have been presmoothed by (3×3)-averaging. In the second pair (Figs. 4 and 6), adjacent sections through the heart region are shown; the images have been obtained via PE tomography. [36] Before processing, the original data have been calibrated with respect to intensity and contrast and smoothed by (3×3)-averaging. Within the third pair (Figs. 7 and 9), which will be used for the experiments with the rigid motion of a subregion, the first image has been artificially generated by selecting a square cutout in the center of Fig. 3, rotating it by an angle of 5 degree and copying it into Fig. 1. The second image is identical with Fig. 3. [37] All images have the size of 128×128 pixels with a frame of 4 pixels width dyed in black.

---

[33] Cf. [Brune/Maurer/Wagner 09], p. 1197 f.

[34] [Plataniotis/Venetsanopoulos 00], pp. 25 ff.

[35] Images courtesy of Prof. R. Stollberger (TU Graz, Institute of Medical Engineering) and Dr. M. Aschauer (Medical University of Graz, Division of Vascular and Interventional Radiology). From a contrast-modulated sequence comprising 150 frames in total, the frames #50 and #51 (with nearly identical modality) have been selected. The data have been used in [Wagner 10] as well.

[36] Images courtesy of Dr. M. Dawood (University of Münster, European Institute of Molecular Imaging), cf. [Dawood/Büther/Lang/Schober/Schäfers 07]. From an unimodal sequence with mutually coinciding image planes, the frames #29 and #30 have been selected. The data have been used in [Wagner 10] as well.

[37] Thus the underlying deformation contains a subregion subjected to a pure rigid motion.

Image pair 1: MR tomography of the kidney region.

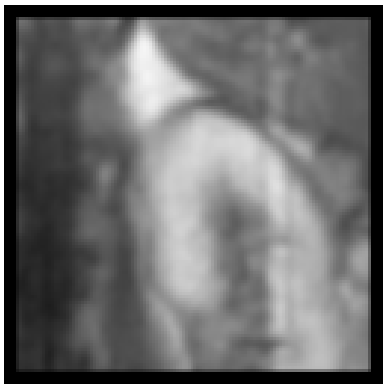

Fig. 1: Template I_1

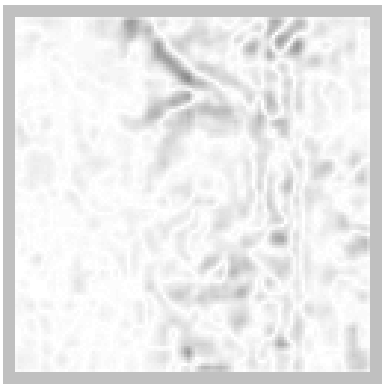

Fig. 2: Grey value difference $|\, I_1 - I_0 \,|$

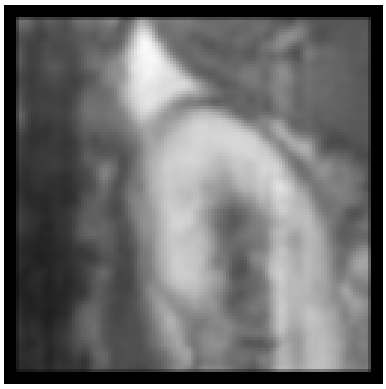

Fig. 3: Reference image I_0

Maximal grey value difference: $\mathrm{Max}_{\,s \,\in\, \Omega} \,|\, I_1(s) - I_0(s) \,| = 0.1529$

Image pair 2: PE tomography of the heart region.

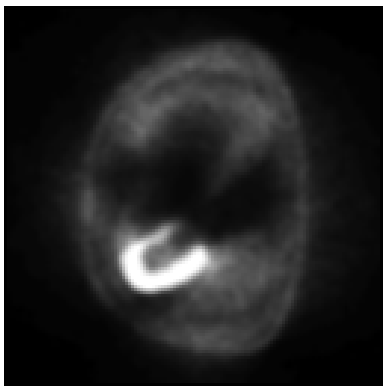

Fig. 4: Template I_1

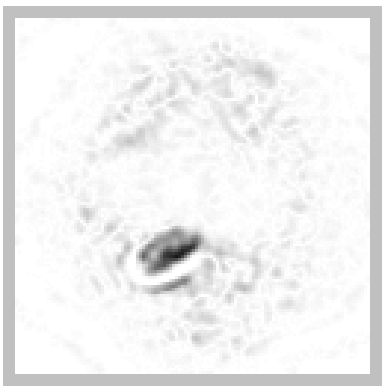

Fig. 5: Grey value difference $|\, I_1 - I_0 \,|$

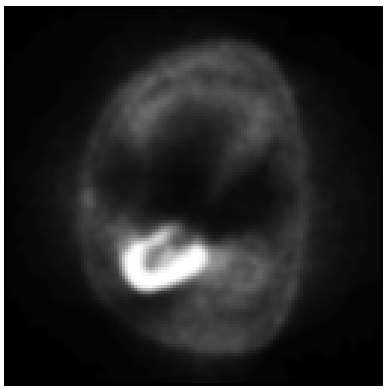

Fig. 6: Reference image I_0

Maximal grey value difference: $\mathrm{Max}_{\,s \,\in\, \Omega} \,|\, I_1(s) - I_0(s) \,| = 0.3019$

Image pair 3: Rotated cutout.

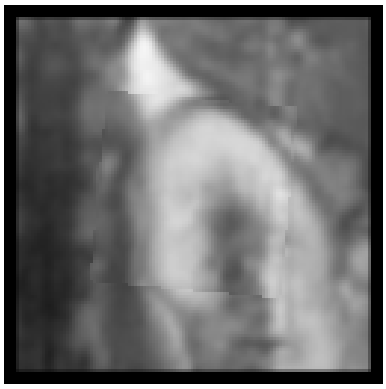

Fig. 7: Template I_1

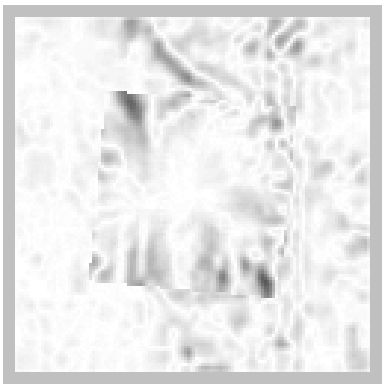

Fig. 8: Grey value difference $|\, I_1 - I_0 \,|$

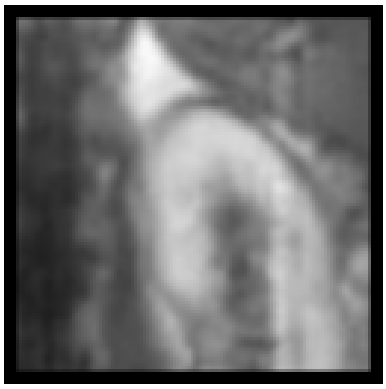

Fig. 9: Reference image I_0

Maximal grey value difference: $\mathrm{Max}_{\,s \,\in\, \Omega} \,|\, I_1(s) - I_0(s) \,| = 0.2196$

b) Experiments with volumetric constraints.

	Image pair 1					
R	$(\mathrm{P})_{lin}$	$(\mathrm{P})_{lin}{}^{(1)}$ $\varepsilon_1 = 10^{-4}$	$(\mathrm{P})_{lin}{}^{(1)}$ $\varepsilon_1 = 10^{-2}$	$(\mathrm{P})_{hyp}$	$(\mathrm{P})_{hyp}{}^{(1)}$ $\varepsilon_1 = 10^{-4}$	$(\mathrm{P})_{hyp}{}^{(1)}$ $\varepsilon_1 = 10^{-2}$
0.5	$Q = 37.8548$ *$G = 0.0329$* $T = 0.000012$	$Q = 37.8529$ *$G = 0.0328$* $T = 0.000051$	$Q = 37.8552$ *$G = 0.0328$* $T = 0.005001$	$Q = 37.4770$ *$G = 0.0353$* $T = 0.000010$	$Q = 37.4771$ *$G = 0.0353$* $T = 0.00051$	$Q = 37.4796$ *$G = 0.0353$* $T = 0.005001$
2.0	$Q = 23.9247$ *$G = 0.0863$* $T = -2.1739$	$Q = 25.0865$ *$G = 0.0715$* $T = 0.00005$	$Q = 25.1961$ *$G = 0.0714$* $T = 0.005$	$Q = 20.1457$ *$G = 0.1028$* $T = -3.4737$	$Q = 22.1639$ *$G = 0.0884$* $T = 0.00005$	$Q = 22.2543$ *$G = 0.0883$* $T = 0.005$
4.0	$Q = 21.8547$ *$G = 0.0914$* $T = -7.8168$	$Q = 22.8772$ *$G = 0.0711$* $T = 0.00005$	$Q = 22.9347$ *$G = 0.0710$* $T = 0.005$	$Q = 15.6321$ *$G = 0.1340$* $T = -6.7668$	$Q = 18.4053$ *$G = 0.0981$* $T = 0.00005$	$Q = 18.4753$ *$G = 0.0979$* $T = 0.005$
8.0	$Q = 20.9248$ *$G = 0.0914$* $T = -7.6112$	$Q = 22.0272$ *$G = 0.0711$* $T = 0.00005$	$Q = 22.0941$ *$G = 0.0710$* $T = 0.005$	$Q = 13.0362$ [a] *$G = 0.1878$* $T = -8.8311$	$Q = 16.1065$ *$G = 0.0988$* $T = 0.00005$	$Q = 16.2547$ *$G = 0.0984$* $T = 0.005$
12.0	$Q = 21.0102$ *$G = 0.0916$* $T = -7.7539$	$Q = 22.0396$ *$G = 0.0709$* $T = 0.00005$	$Q = 22.1089$ *$G = 0.0710$* $T = 0.005$	$Q = 12.9879$ [a] *$G = 0.1954$* $T = -8.1379$	$Q = 16.1856$ *$G = 0.0988$* $T = 0.00005$	$Q = 16.2519$ *$G = 0.0984$* $T = 0.005$

Table 4.1. Variation in R for $\mu = 10^{-5}$, $\eta_{max} = 0.001$. In $(\mathrm{P})_{hyp}$ and $(\mathrm{P})_{hyp}{}^{(1)}$, $p = 2$, $c_1 = 0.05$, $c_2 = 0.25$ have been chosen.

	Image pair 2					
R	$(\mathrm{P})_{lin}$	$(\mathrm{P})_{lin}{}^{(1)}$ $\varepsilon_1 = 10^{-4}$	$(\mathrm{P})_{lin}{}^{(1)}$ $\varepsilon_1 = 10^{-2}$	$(\mathrm{P})_{hyp}$	$(\mathrm{P})_{hyp}{}^{(1)}$ $\varepsilon_1 = 10^{-4}$	$(\mathrm{P})_{hyp}{}^{(1)}$ $\varepsilon_1 = 10^{-2}$
0.5	$Q = 34.50838$ *$G = 0.0230$* $T = 0.000043$	$Q = 34.5038$ *$G = 0.0230$* $T = 0.000061$	$Q = 34.5044$ *$G = 0.0230$* $T = 0.005003$	$Q = 34.1488$ *$G = 0.0211$* $T = 0.000036$	$Q = 34.1490$ *$G = 0.0211$* $T = 0.000058$	$Q = 34.1500$ *$G = 0.0211$* $T = 0.005003$
2.0	$Q = 21.9221$ *$G = 0.0755$* $T = -2.6858$	$Q = 22.4079$ *$G = 0.0468$* $T = 0.00005$	$Q = 22.4269$ *$G = 0.0466$* $T = 0.005001$	$Q = 18.6264$ *$G = 0.0772$* $T = -3.4417$	$Q = 19.7118$ *$G = 0.0576$* $T = 0.00005$	$Q = 19.7637$ *$G = 0.0572$* $T = 0.005001$
4.0	$Q = 18.5002$ *$G = 0.0798$* $T = -4.0353$	$Q = 19.1647$ *$G = 0.0422$* $T = 0.00005$	$Q = 19.1864$ *$G = 0.0418$* $T = 0.005001$	$Q = 12.7733$ *$G = 0.0756$* $T = -4.0734$	$Q = 14.7114$ *$G = 0.0444$* $T = 0.00005$	$Q = 14.7809$ *$G = 0.0435$* $T = 0.005001$
8.0	$Q = 18.1730$ [b] *$G = 0.0797$* $T = -4.2868$	$Q = 18.8974$ [c] *$G = 0.0396$* $T = 0.00005$	$Q = 18.8928$ *$G = 0.0422$* $T = 0.005001$	$Q = 11.4767$ [d] *$G = 0.0852$* $T = -5.2111$	$Q = 13.7393$ [e] *$G = 0.0485$* $T = 0.00005$	$Q = 13.7776$ *$G = 0.0479$* $T = 0.005$
12.0	$Q = 18.1807$ *$G = 0.0797$* $T = -4.2868$	$Q = 18.8908$ *$G = 0.0424$* $T = 0.00005$	$Q = 18.9233$ *$G = 0.0396$* $T = 0.005$	$Q = 11.3974$ *$G = 0.0852$* $T = -5.5780$	$Q = 13.6216$ [a] *$G = 0.0468$* $T = 0.00005$	$Q = 13.7730$ *$G = 0.0501$* $T = 0.005$

Table 4.2. Variation in R for $\mu = 10^{-5}$, $\eta_{max} = 0.001$. In $(\mathrm{P})_{hyp}$ and $(\mathrm{P})_{hyp}{}^{(1)}$, $p = 2$, $c_1 = 0.05$, $c_2 = 0.25$ have been chosen.

We provide three series of results for the problems $(\mathrm{P})_{lin}{}^{(1)}$ and $(\mathrm{P})_{hyp}{}^{(1)}$ with the volumetric constraint (2.7) and $\Theta = \Omega$. In the first and second series, the influence of the parameter R has been studied while in the third series, R is kept constant but ε_1 varies. For comparison, the problems $(\mathrm{P})_{lin}$ and $(\mathrm{P})_{hyp}$ have been solved as well.

	Image pair 1			
ε_1	$(\mathrm{P})_{lin}$	$(\mathrm{P})_{lin}{}^{(1)}$	$(\mathrm{P})_{hyp}$	$(\mathrm{P})_{hyp}{}^{(1)}$
(2.7) not present	$Q = 13.2374$ [a) b)] *G= 0.1500* $T = -17.3888$		$Q = 12.9879$ [a)] *G= 0.1954* $T = -8.1379$	
10^{-6}		$Q = 16.4122$ *G= 0.0937* $T = 10^{-6}$		$Q = 16.1747$ *G= 0.0988* $T = 10^{-6}$
10^{-5}		$Q = 16.4178$ *G= 0.0936* $T = 0.000005$		$Q = 16.1750$ *G= 0.0988* $T = 0.000005$
10^{-4}		$Q = 16.4372$ *G= 0.0936* $T = 0.00005$		$Q = 16.1856$ *G= 0.0988* $T = 0.00005$
10^{-3}		$Q = 16.4532$ *G= 0.0937* $T = 0.0005$		$Q = 16.1971$ *G= 0.0987* $T = 0.0005$
10^{-2}		$Q = 16.5181$ [c)] *G= 0.0937* $T = 0.005$		$Q = 16.2519$ *G= 0.0984* $T = 0.005$
10^{-1}		$Q = 17.1819$ *G= 0.0927* $T = 0.050001$		$Q = 16.9397$ *G= 0.0956* $T = 0.050001$
0.50		$Q = 22.0640$ *G= 0.0733* $T = 0.25$		$Q = 21.8621$ *G= 0.0782* $T = 0.25$

Table 4.3. Variation in ε_1 for $R = 12$, $\eta_{max} = 0.001$. In $(\mathrm{P})_{lin}$ and $(\mathrm{P})_{lin}{}^{(1)}$, we used $\mu = 10^{-6}$. In $(\mathrm{P})_{hyp}$ and $(\mathrm{P})_{hyp}{}^{(1)}$, $\mu = 10^{-5}$, $p = 2$, $c_1 = 0.05$, $c_2 = 0.25$ have been chosen.

Remarks. Table 4.1.: a) G exceeds the maximal grey value difference of the original images.
Table 4.2.: a) Best value obtained in presence of (2.7) at all. b) See Figs. $16-19$. c) See Figs. $20-22$. d) See Figs. $23-25$. e) See Figs. $26-28$.
Table 4.3.: a) G exceeds the maximal grey value difference of the original images. b) See Figs. 10, 11 and 14. c) See Figs. 12, 13 and 15.

c) The control restriction as a regularization parameter.

Already in [Brune/Maurer/Wagner 09] and [Wagner 10], it has been pointed out that the introduction of a gradient constraint has a regularizing effect by itself. This statement will be supported again by quantitative results obtained with $(\mathrm{P})_{lin}{}^{(1)}$ and $(\mathrm{P})_{hyp}{}^{(1)}$. In the following experiments, we use again the image pair 1 and vary R exclusively while all other parameters have been kept constant.

	Image pair 1	
R	$(\mathrm{P})_{lin}{}^{(1)}$	$(\mathrm{P})_{hyp}{}^{(1)}$
0.50	$Q = 40.7873$	$Q = 40.4265$
0.75	$Q = 35.7710$	$Q = 34.9613$
1.00	$Q = 33.0452$	$Q = 31.7624$
2.00	$Q = 29.2175$	$Q = 26.5697$
4.00	$Q = 27.0962$	$Q = 22.9474$
8.00	$Q = 25.9010$	$Q = 20.3595$
12.00	$Q = 25.7438$ [a)]	$Q = 20.1982$
16.00	$Q = 25.7476$	$Q = 20.1643$ [a)]
32.00	$Q = 25.8166$	$Q = 20.1946$
10^2	$Q = 25.9233$	$Q = 20.4197$
10^3	$Q = 25.7812$	$Q = 20.2477$ [b)]
10^4	$Q = 25.7812$	$Q = 20.2477$
10^5	$Q = 25.7789$ [c)]	$Q = 20.3781$
10^6	$Q = 25.7789$	$Q = 20.2216$

Remarks. a) Best registration within this column. b) Another local minimum of $Q(\hat{x}, \hat{y})$. c) By further increase of R, neither the optimal solution of $(\mathrm{P})_{lin}{}^{(1)}$ nor $Q(\hat{x}, \hat{y})$ will be changed.

Table 4.4. Regularizing effect of R with $\mu = 10^{-5}$, $\eta_{max} = 10^{-5}$, $\varepsilon_1 = 10^{-4}$. In $(\mathrm{P})_{hyp}{}^{(1)}$, $p = 2$, $c_1 = 0.05$, $c_2 = 0.25$ have been chosen. In all experiments, we obtained $G \leqslant 0.02$.

d) Experiments with rigid motion of a subregion.

In this subsection, we present selected results for the problems $(\mathrm{P})_{lin}{}^{(2)}$ and $(\mathrm{P})_{hyp}{}^{(2)}$. The additional restrictions (2.10) and (2.11) have been imposed in the subregion $\Theta = [\,30\,,\,96\,]^2$, which corresponds with the rotated cutout of Fig. 3.

	Image pair 3			
R	$(\mathrm{P})_{lin}$	$(\mathrm{P})_{lin}{}^{(2)}$	$(\mathrm{P})_{hyp}$	$(\mathrm{P})_{hyp}{}^{(2)}$
0.5	$Q = 31.6158$ *G= 0.0232*	$Q = 43.5790$ *G= 0.0234*	$Q = 31.3315$ *G= 0.0241*	$Q = 43.4407$ *G= 0.0241*
2.0	$Q = 20.7947$ *G= 0.0863*	$Q = 32.1040$ *G= 0.0863*	$Q = 18.1770$ *G= 0.1028*	$Q = 30.8851$ *G= 0.1028*
4.0	$Q = 19.3102$ *G= 0.0908*	$Q = 30.9771$ *G= 0.0908*	$Q = 14.7338$ *G= 0.1340*	$Q = 29.0481$ *G= 0.1340*
8.0	$Q = 19.0335$ [b)] *G= 0.0914*	$Q = 30.8352$ [c)] *G= 0.0914*	$Q = 12.8937$ [a) d)] *G= 0.2285*	$Q = 28.2273$ [e)] *G= 0.2029*
12.0	$Q = 19.0317$ *G= 0.0916*	$Q = 30.7804$ *G= 0.0914*	$Q = 12.7180$ [a)] *G= 0.3750*	$Q = 28.1374$ [a)] *G= 0.2793*
16.0	$Q = 19.0612$ *G= 0.0811*	$Q = 30.8155$ *G= 0.0578*	$Q = 12.8120$ [a)] *G= 0.4615*	$Q = 28.1683$ [a)] *G= 0.4105*

Table 4.5. Rigid motion of $\Theta = [\,33\,,\,96\,]^2$ for $\mu = 10^{-5}$, $\eta_{max} = 0.001$ and $\varepsilon = 10^{-4}$. In $(\mathrm{P})_{hyp}$ and $(\mathrm{P})_{hyp}{}^{(2)}$, $p = 2$, $c_1 = 0.05$, $c_2 = 0.25$ have been chosen.

Remarks. a) G exceeds the maximal grey value difference of the original images. b) See Figs. $28-30$. c) See Figs. $31-33$. d) See Figs. $34-36$. e) See Figs. $37-39$.

e) Figures.

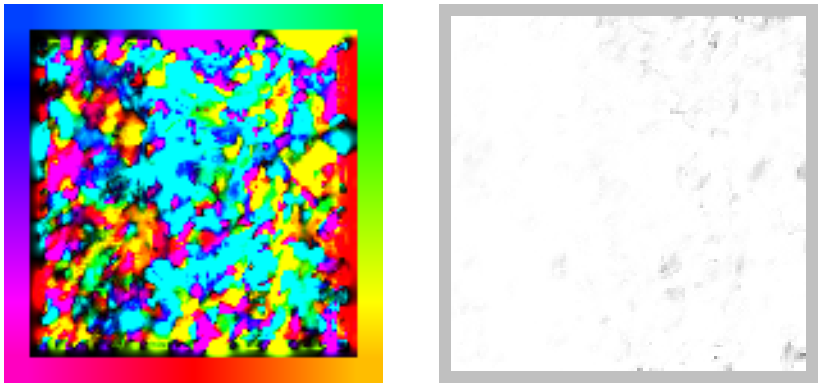

Figs. $10-11$: Results for $(\mathrm{P})_{lin}$ and image pair 1 with $\mu = 10^{-6}$, $\eta_{max} = 0.001$ and $R = 12.0$

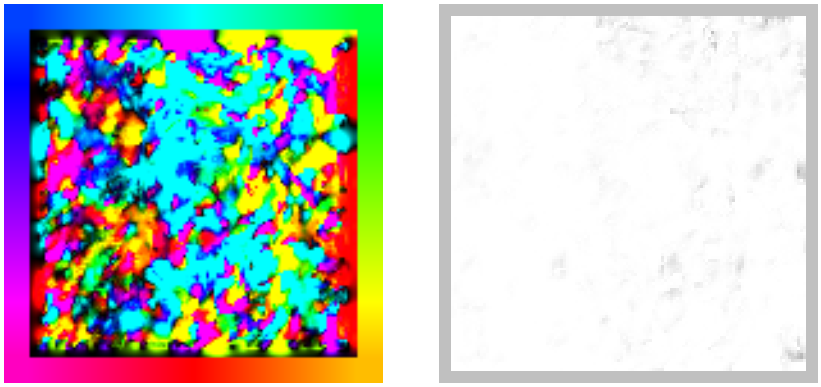

Figs. $12-13$: Results for $(\mathrm{P})_{lin}{}^{(1)}$ and image pair 1 with $\mu = 10^{-6}$, $\eta_{max} = 0.001$, $\varepsilon_1 = 0.01$ and $R = 12.0$

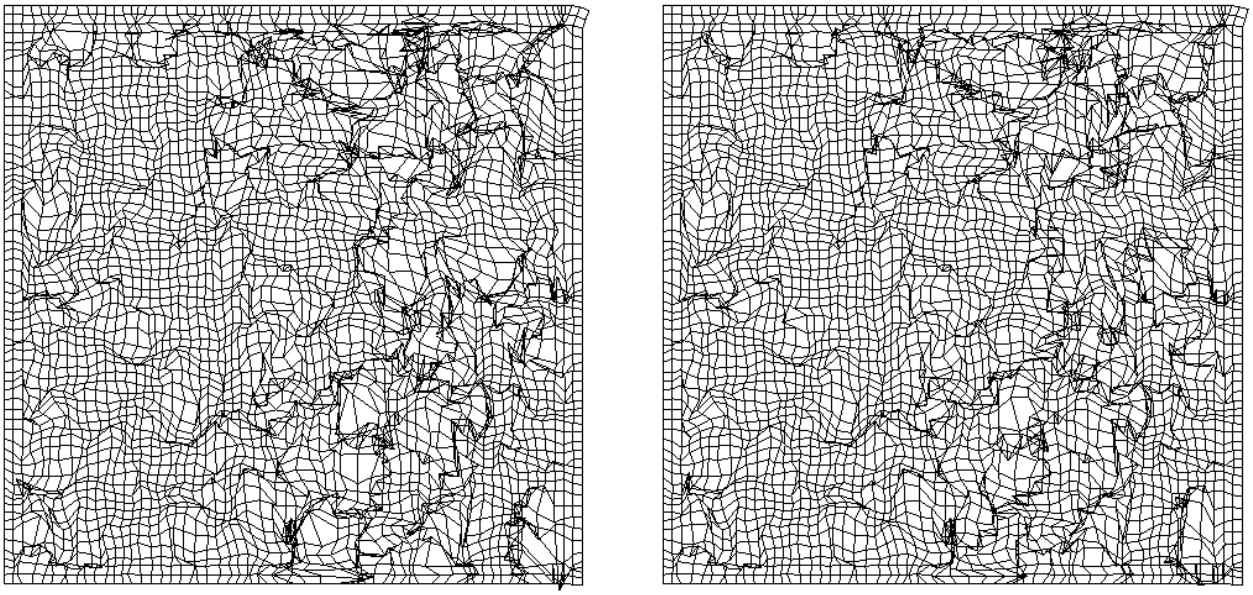

Figs. $14-15$: Deformed grids for the experiments above. Left: result of $(\mathrm{P})_{lin}$. Right: result of $(\mathrm{P})_{lin}{}^{(1)}$.

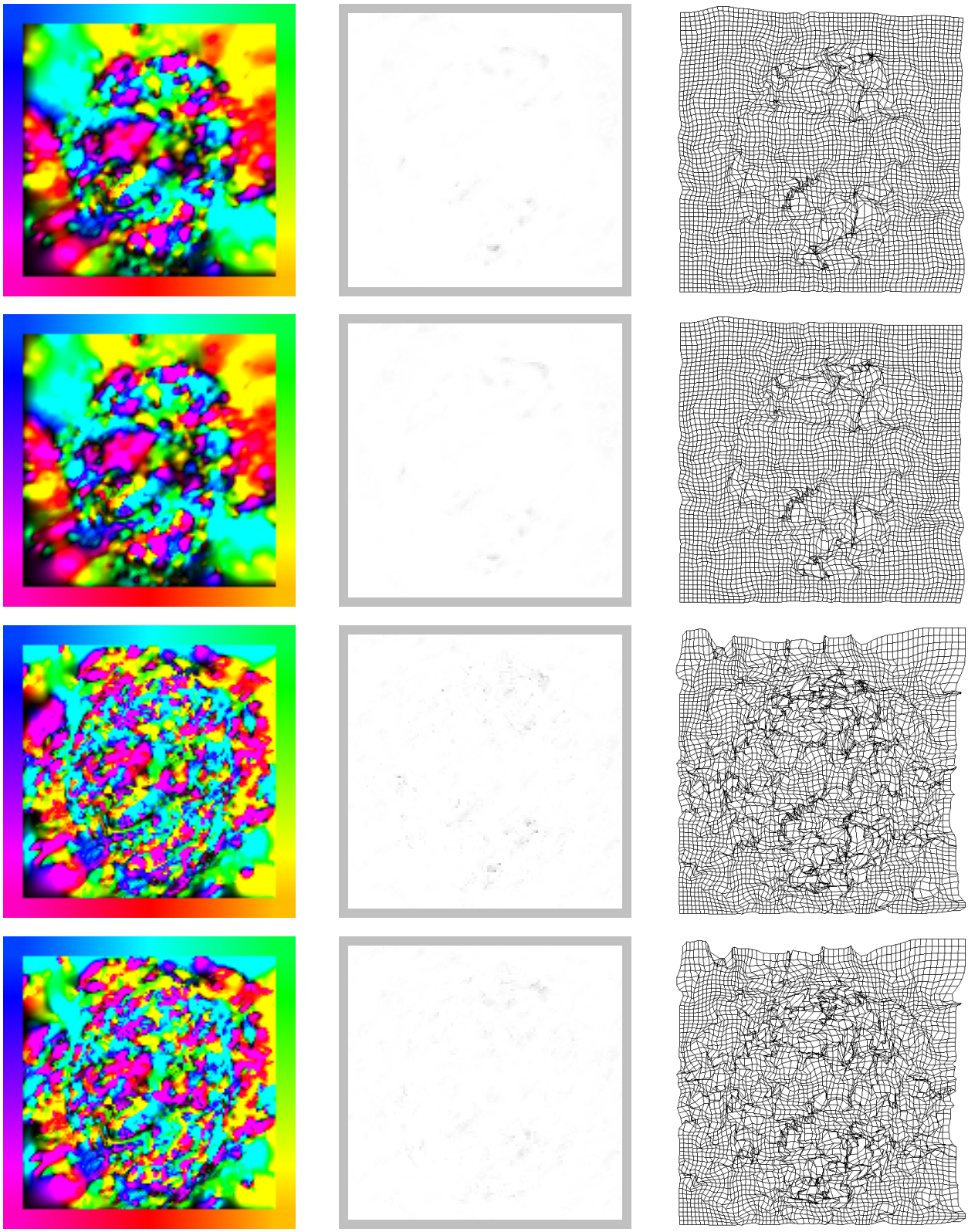

Figs. 16 – 27: Results for image pair 2 with $\mu = 10^{-5}$, $\eta_{max} = 0.001$ and $R = 8.0$. First row: $(\mathrm{P})_{lin}$. Second row: $(\mathrm{P})_{lin}{}^{(1)}$ with $\varepsilon_1 = 10^{-4}$. Third row: $(\mathrm{P})_{hyp}$ with $p = 2$, $c_1 = 0.05$, $c_2 = 0.25$. Fourth row: $(\mathrm{P})_{hyp}{}^{(1)}$ with $p = 2$, $c_1 = 0.05$, $c_2 = 0.25$ and $\varepsilon_1 = 10^{-4}$.

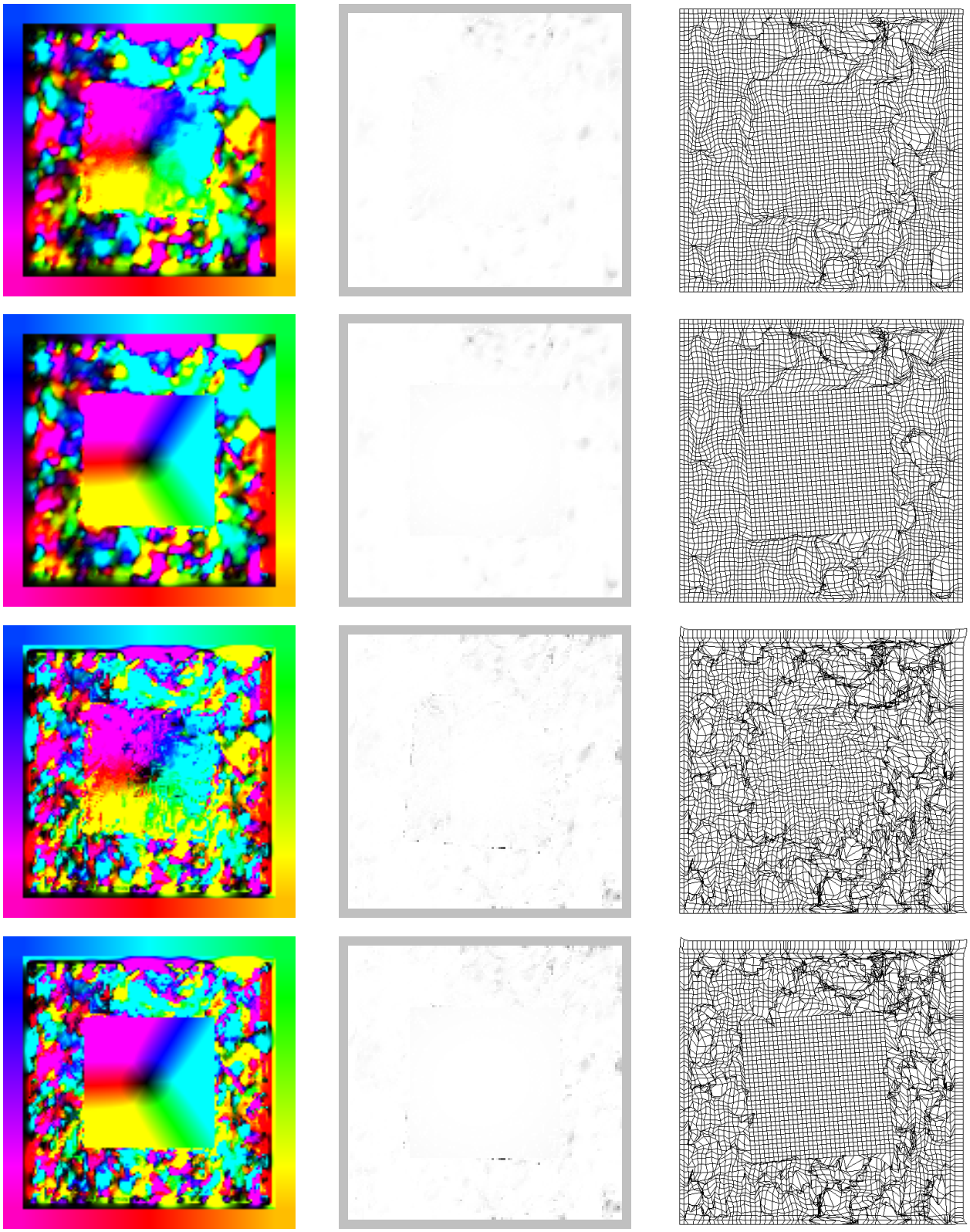

Figs. 28 – 39: Results for image pair 3 with $\mu = 10^{-5}$, $\eta_{max} = 0.001$ and $R = 8.0$. First row: $(\mathrm{P})_{lin}$. Second row: $(\mathrm{P})_{lin}{}^{(1)}$ with $\varepsilon = 10^{-4}$. Third row: $(\mathrm{P})_{hyp}$ with $p = 2$, $c_1 = 0.05$, $c_2 = 0.25$. Fourth row: $(\mathrm{P})_{hyp}{}^{(1)}$ with $p = 2$, $c_1 = 0.05$, $c_2 = 0.25$ and $\varepsilon = 10^{-4}$.

5. Discussion and conclusions.

The experiments with $(\mathrm{P})_{lin}{}^{(1)}$ and $(\mathrm{P})_{hyp}{}^{(1)}$ in Subsect. 4.b) show that, with an appropriate choice of the parameters μ, η_{max} and R, the registration will reduce the relative error by $80-85\%$ even in presence of the volumetric constraint (2.7). The best value amounts to $Q = 13.62\%$. For identical values of μ, R and η_{max}, the hyperelastic regularization produces always the better values of Q. This will be confirmed even by Table 4.3. where in $(\mathrm{P})_{lin}{}^{(1)}$ a smaller regularization parameter μ has been used than in $(\mathrm{P})_{hyp}{}^{(1)}$. On the other hand, as one may expect, the problem $(\mathrm{P})_{lin}{}^{(1)}$ is superior to $(\mathrm{P})_{hyp}{}^{(1)}$ with respect to the runtime behaviour.
In the direct comparison of $(\mathrm{P})_{lin}{}^{(1)}$ and $(\mathrm{P})_{hyp}{}^{(1)}$ with the problems $(\mathrm{P})_{lin}$ and $(\mathrm{P})_{hyp}$, we observe a loss of no more than $1-3\%$ of registration quality while the — sometimes severe — grid tangling from $(\mathrm{P})_{lin}$ and $(\mathrm{P})_{hyp}$ has been completely removed (compare, e. g., Figs. 14 and 15 with $T = -17.388$ and $T = 0.005$, respectively). Further, in all experiments with $(\mathrm{P})_{lin}{}^{(1)}$ and $(\mathrm{P})_{hyp}{}^{(1)}$, the grey value correction G is systematically smaller than in $(\mathrm{P})_{lin}$ and $(\mathrm{P})_{hyp}$, remaining always below the maximal grey value difference of the original images. The variation of the parameter ε_1 within $[\,10^{-5}\,,\,10^{-2}\,]$ causes only minor changes of the reconstruction quality. A noticeable effect will not be obtained until $\varepsilon_1 \approx 0.1$, then resulting in a heavy smoothing of the deformation and a substantial loss of reconstruction quality.
The results of Subsection 4.c) demonstrate that, within $(\mathrm{P})_{lin}{}^{(1)}$ and $(\mathrm{P})_{hyp}{}^{(1)}$, the parameter R from the control restriction behaves like an additional regularization parameter since the reconstruction quality reaches its minimum for values $R \in [\,12\,,\,16\,]$.
Our experiments with $(\mathrm{P})_{lin}{}^{(2)}$ and $(\mathrm{P})_{hyp}{}^{(2)}$ in Subsect. 4.d) show the possibility to detect simultaneously an overall elastic deformation and a rigid motion of a subregion known in advance. The incorporation of the corresponding constraints becomes important if, on the base of $\hat{x}$, conclusions about the actual motion of the pictured objects will be drawn. Then the motions known in advance should be replicated within $\hat{x}$. Observe that the solutions of $(\mathrm{P})_{lin}$ and $(\mathrm{P})_{hyp}$ give only a "hint" for the rotating motion of the central part without determining the rotation exactly. The loss of reconstruction quality in the results of $(\mathrm{P})_{lin}{}^{(2)}$ and $(\mathrm{P})_{hyp}{}^{(2)}$ may be attributed to the incompatibility between rotation and elastic deformation at the border $\partial\Theta$, which will be indicated by the plots of the greyscale correction as well (see Figs. 35 and 38).

Conclusion.

In the present work, we demonstrated that the elastic/hyperelastic image registration problem can be successfully reformulated and solved as a multidimensional control problem with convex and polyconvex constraints. In accordance with the requirements of the registration and the a priori available information, the problems can be augmented with additional state and control restrictions, to the point of modelling the rigid motion of selected subregions. In presence of the volumetric constraint (2.7), the relative error between template and reference image could be reduced in the course of the registration by up to 85% while grid tangling has been completely suppressed. Consequently, it seems advisable to keep the constraint (2.7) in future applications.

Acknowledgement.

The author wishes to thank the participants of the workshop "Optimal Control in Image Processing" for stimulating discussions. Further, he would like to thank Prof. R. Stollberger (Graz), M. Aschauer (Graz) and M. Dawood (Münster) who kindly provided me with tomographic image data. This work has been supported within the Special Research Unit "Mathematical Optimization and Applications in Biomedical Sciences" (Graz) by the Austrian Science Fund.

References.

1. [Alvarez/Weickert/Sánchez 00] Alvarez, L.; Weickert, J.; Sánchez, J.: *Reliable estimation of dense optical flow fields with large displacements.* Int. J. Computer Vision **39** (2000), 41 – 56
2. [Aubert/Kornprobst 06] Aubert, G.; Kornprobst, P.: *Mathematical Problems in Image Processing: Partial Differential Equations and the Calculus of Variations.* Springer; New York etc. 2006, 2nd ed.
3. [Ball 77] Ball, J. M.: *Convexity conditions and existence theorems in nonlinear elasticity.* Arch. Rat. Mech. Anal. **63** (1977), 337 – 403
4. [Barbieri/Welk/Weickert 09] Barbieri, S.; Welk, M.; Weickert, J.: *A variational approach to the registration of tensor-valued images.* In: Aja-Fernández, S.; de Luis-García, R.; Tao, D.; Li, X. (Eds.): Tensors in Image Processing and Computer Vision. Springer; London etc. 2009, 59 – 77
5. [Berger 04] Berger, M.: *Geometry I.* Springer; Berlin etc. 2004, 3rd, corrected ed.
6. [Breitenreicher/Schnörr 09] Breitenreicher, D.; Schnörr, C.: *Robust 3D object registration without explicit correspondence using geometric integration.* Machine Vis. and Appl.; electronically published: http://dx.doi.org/10.1007/s00138-009-0227-6 (accessed at 01. 12. 2009)
7. [Broit 81] Broit, C.: *Optimal registration of deformed images.* PhD thesis. University of Pennsylvania, Philadelphia 1981
8. [Brune/Maurer/Wagner 09] Brune, C.; Maurer, H.; Wagner, M.: *Detection of intensity and motion edges within optical flow via multidimensional control.* SIAM J. Imaging Sci. **2** (2009), 1190 – 1210
9. [Chmelka/Melan 76] Chmelka, F.; Melan, E.: *Einführung in die Festigkeitslehre.* Springer; Wien - New York 1976, 5th ed.
10. [Christensen/Rabbitt/Miller 96] Christensen, G. E.; Rabbitt, R. D.; Miller, M. I.: *Deformable templates using large deformation kinematics.* IEEE Trans. Image Processing **5** (1996), 1435 – 1447
11. [Dacorogna 08] Dacorogna, B.: *Direct Methods in the Calculus of Variations.* Springer; New York etc. 2008, 2nd ed.
12. [Dacorogna/Ribeiro 06] Dacorogna, B.; Ribeiro, A. M.: *On some definitions and properties of generalized convex sets arising in the calculus of variations.* In: Chipot, M.; Ninomiya, H. (Eds.): Recent Advances on Elliptic and Parabolic Issues. Proceedings of the 2004 Swiss-Japanese Seminar: Zurich, Switzerland, 6-10 December 2004. World Scientific; New Jersey etc. 2006, 103 – 128
13. [Dawood/Büther/Lang/Schober/Schäfers 07] Dawood, M.; Büther, F.; Lang, N.; Schober, O.; Schäfers, K. P.: *Respiratory gating in positron emission tomography: a quantitative comparision of different gating schemes.* Med. Phys. **34** (2007), 3067 – 3076
14. [Droske/Rumpf 04] Droske, M.; Rumpf, M.: *A variational approach to nonrigid morphological image registration.* SIAM J. Appl. Math. **64** (2004), 668 – 687
15. [Droske/Rumpf 07] Droske, M.; Rumpf, M.: *Multiscale joint segmentation and registration of image morphology.* IEEE Trans. Pattern Recognition Machine Intelligence **29** (2007), 2181 – 2194
16. [Evans/Gariepy 92] Evans, L. C.; Gariepy, R. F.: *Measure Theory and Fine Properties of Functions.* CRC Press; Boca Raton etc. 1992
17. [Fischer/Modersitzki 03] Fischer, B.; Modersitzki, J.: *Curvature based image registration.* J. Math. Imaging Vision **18** (2003), 81 – 85
18. [Fourer/Gay/Kernighan 03] Fourer, R.; Gay, D. M.; Kernighan, B. W.: *AMPL. A Modeling Language for Mathematical Programming.* Brooks/Cole — Thomson Learning; Pacific Grove 2003, 2nd ed.
19. [Franek/Franek/Maurer/Wagner 10] Franek, L.; Franek, M.; Maurer, H.; Wagner, M.: *A discretization method for the numerical solution of Dieudonné-Rashevsky type problems with application to edge detection within noisy image data.* KFU Graz, SFB-Report No. 2010–030. Submitted: Opt. Contr. Appl. Meth.
20. [Gasser/Holzapfel 02] Gasser, T. C.; Holzapfel, G. H.: *A rate-independent elastoplastic constitutive model for biological fiber-reinforced composites at finite strains: continuum basis, algorithmic formulation and finite element implementation.* Computational Mechanics **29** (2002), 340 – 360
21. [Haber/Modersitzki 04] Haber, E.; Modersitzki, J.: *Numerical methods for volume preserving image registration.* Inverse Problems **20** (2004), 1621 – 1638
22. [Haber/Modersitzki 07] Haber, E.; Modersitzki, J.: *Image registration with guaranteed displacement regularity.* Int. J. Computer Vision **71** (2007), 361 – 372
23. [Haker/Zhu/Tannenbaum/Angenent 04] Haker, S.; Zhu, L.; Tannenbaum, A.; Angenent, S.: *Optimal mass transport for registration and warping.* Int. J. Computer Vision **60** (2004), 225 – 240
24. [Haussecker/Fleet/Jähne/Garbe/Scharr/Spies 09] Haußecker, H.; Fleet, D.; Jähne, B.; Garbe, C..; Scharr, H.; Spies, H.: *A new framework for image sequence analysis: optical flow with physics-based brightness*

models. To appear in: Jähne, B.; Garbe, C. S. (Eds.): Image Sequence Analysis to Investigate Dynamic Processes. Springer; Berlin etc.

25. [Henn/Witsch 00] Henn, S.; Witsch, K.: *A multigrid approach for minimizing a nonlinear functional for digital image matching.* Computing **64** (2000), 339 – 348
26. [Henn/Witsch 01] Henn, S.; Witsch, K.: *Iterative multigrid regularization techniques for image matching.* SIAM J. Sci. Comput. **23** (2001), 1077 – 1093
27. [Hintermüller/Keeling 09] Hintermüller, M.; Keeling, S. L.: *Image registration and segmentation based on energy minimization.* In: Pardalos, P. M.; Romeijn, H. E. (Eds.): Handbook of Optimization in Medicine. Springer; New York 2009, 213 – 252
28. [Jansen 97] Jansen, B.: *Interior Point Techniques in Optimization.* Kluwer; Dordrecht 1997
29. [Keeling/Ring 05] Keeling, S. L.; Ring, W.: *Medical image registration and interpolation by optical flow with maximal rigidity.* J. Math. Imaging Vision **23** (2005), 47 – 65
30. [Laird/Wächter 09] Laird, C.; Wächter, A.: *Introduction to IPOPT: A tutorial for downloading, installing, and using IPOPT. Revision No. 1690.* Electronically published: http://www.coin-or.org/Ipopt/documentation/ (accessed at 17. 09. 2010)
31. [Le Guyader/Vese 09] Le Guyader, C.; Vese, L.: *A combined segmentation and registration framework with a nonlinear elasticity smoother.* In: Tai, X.-C.; Mørken, K.; Lysaker, M.; Lie, K.-A. (Eds.): Scale Space and Variational Methods in Computer Vision, Second International Conference, SSVM 2009, Voss, Norway, June 1-5, 2009. Proceedings. Springer; Berlin - Heidelberg 2009 (LNCS 5567), 600 – 611
32. [Modersitzki 04] Modersitzki, J.: *Numerical Methods for Image Registration.* Oxford University Press; Oxford 2004
33. [Modersitzki 09] Modersitzki, J.: *FAIR. Flexible Algorithms for Image Registration.* SIAM; Philadelphia 2009
34. [Museyko/Stiglmayr/Klamroth/Leugering 09] Museyko, O.; Stiglmayr, M.; Klamroth, K.; Leugering, G.: *On the application of the Monge-Kantorovich problem to image registration.* SIAM J. Imaging Sci. **2** (2009), 1068 – 1097
35. [Ogden 03] Ogden, R. W.: *Nonlinear elasticity, anisotropy, material stability and residual stresses in soft tissue.* In: Holzapfel, G. A.; Ogden, R. W. (Eds.): Biomechanics of Soft Tissue in Cardiovascular Systems. Springer; Wien etc. 2003, 65 – 108
36. [Plataniotis/Venetsanopoulos 00] Plataniotis, K. N.; Venetsanopoulos, A. N.: *Color Image Processing and Applications.* Springer; Berlin etc. 2000
37. [Pöschl/Modersitzki/Scherzer 10] Pöschl, C.; Modersitzki, J.; Scherzer, O.: *A variational setting for volume constrained image registration.* Inverse Probl. Imaging **4** (2010), 505 – 522
38. [Ruhnau/Schnörr 07] Ruhnau, P.; Schnörr, C.: *Optical Stokes flow estimation: an imaging-based control approach.* Experiments in Fluids **42** (2007), 61 – 78
39. [Scherzer/Grasmair/Grossauer/Haltmeier/Lenzen 09] Scherzer, O.; Grasmair, M.; Grossauer, H.; Haltmeier, M.; Lenzen, F.: *Variational Methods in Imaging.* Springer; New York etc. 2009
40. [Vemuri/Ye/Chen/Leonard 00] Vemuri, B. C.; Ye, J.; Chen, Y.; Leonard, C. M.: *A level-set based approach to image registration.* In: IEEE Workshop on Mathematical Methods in Biomedical Image Analysis (MMBIA'00). IEEE Computer Society; Washington 2000, 86 – 93
41. [Wächter/Biegler 06] Wächter, A.; Biegler, L. T.: *On the implementation of an interior-point filter line-search algorithm for large-scale nonlinear programming.* Math. Program. Ser. A **106** (2006), 25 – 57
42. [Wagner 08] Wagner, M.: *Quasiconvex relaxation of multidimensional control problems with integrands $f(t, \xi, v)$.* Max-Planck-Institut für Mathematik in den Naturwissenschaften, Leipzig. Preprint 68/2008. Accepted for publication: ESAIM: Control, Optimisation and Calculus of Variations
43. [Wagner 09] Wagner, M.: *Pontryagin's maximum principle for multidimensional control problems in image processing.* J. Optim. Theory Appl. **140** (2009), 543 – 576
44. [Wagner 10] Wagner, M.: *An optimal control approach to the elastic/hyperelastic image registration problem.* University of Graz, SFB-Report No. 2010–031

Last modification: 20. 09. 2010

Author's address: Marcus Wagner, University of Graz, Institute for Mathematics and Scientific Computing, Heinrichstraße 36, A-8010 Graz, Austria.

Homepage / e-mail: `www.thecitytocome.de` / `marcus.wagner@uni-graz.at`